2015

A Computational Model of Cell Movement Linked to Substrate Rigidity

Jie Sheng
Lehigh University

A Computational Model of Cell Movement Linked to Substrate Rigidity

by

Jie Sheng

A Thesis

Presented to the Graduate and Research Committee

of Lehigh University

in Candidacy for the Degree of

Master of Science

in

Mechanical Engineering and Mechanics

Lehigh University

May, 2015

This thesis is accepted and approved in partial fulfillment of requirements for the Master of Science.

_____

Date Approved

_____

Dr. Arkady Voloshin, Thesis Advisor

_____

Dr. D. Gary Harlow, Chairperson of Department

ACKNOWLEDGEMENTS

I would like to highly thank my advisor, Dr. Arkady Voloshin, for his continued patience and valuable guidance. Dr. Voloshin let me learn not only the attitude for academic research but also rules of working as an outstanding graduate student. I would also like to thank Mrs. Xingyue Zhang, Mr. Xue Xiao, Mr. Shuoran Du and Dr. Tianyi Luo for their generous help and support.

Finally, my special thanks to my parents and my family, for their continuous support, understanding and encouragement.

TABLE OF CONTENTS

LIST OF TABLES

LIST OF FIGURES

ABSTRACT

Living cells as physical entities can response the changes of the physiological environment as well as mechanical stimuli occurring in and out of the cell body. It is well documented that cell directional motion is determined by the substrate stiffness. Cells tend to move towards stiffer substrate. Cytoskeleton plays a significant role in intracellular force equilibrium and extracellular force balance between substrate and cell via focal adhesions.

Cellular deformations can be evaluated by the use of computational models. In this thesis, a finite element modelling approach that describes the biomechanical behaviors of cells is presented. We model cytoskeleton as a tensegrity structure and substrate as a spring element. The tensegrity structure has many features that are capable to model behavior of a living cell. The structure consists of tension-supporting cables and compression-supporting struts that represent the microfilaments and microtubules, respectively. The effects of substrate stiffness and prestress on strain energy of a cell are investigated by defining several substrate stiffness values and prestress values. The model is placed on a flat surface, which represents a cell anchored to an elastic substrate via focal adhesions. Numerical simulation results reveal that the strain energy of the whole cell decreases as substrate stiffness increases. As prestress of cell increases, the strain energy increases. The change of prestress value does not change behavior pattern of the strain energy: cell's strain

energy will decrease when substrate stiffness increases. The findings indicate that both cell prestress and substrate stiffness have certain influences on cells' directional movements and structural deformations.

1 Introduction

Mechanical stimulation is known to cause cell's morphology changes when they are adhering to a substrate. The mechanisms by which different environmental forces are transduced into cell biological responses are still unknown. In any physical environment, changes of cell's geometry and motion are influenced by its physical and internal balance [1] since a cell needs to maintain its morphological stability and molecular self-assembly. Cell adhering to a substrate can sense mechanical stimuli [2,3,4], respond the stimuli in order to keep cell's intracellular and extracellular forces in balance [5,6], and regulate many important physiological and pathological processes [7,8,9].

Current experimental work focuses on developing and identifying the mechanism called "mechanotransduction", the processes by which cells sense mechanical force and transduce it into a biochemical signal. Some of these studies have shown that cell movements have been influenced by substrate rigidity [10,11]. Based on the hypothesis that single cell can probe substrate stiffness and respond by exerting contractile forces, Lo and colleagues [10] referred to the process as "durotaxis". On the other hand, both computational [12,13,14] and mathematical models [15] have been developed for further understanding of the biomechanical cellular responses. Computational mechanical models, especially tensegrity structures [16,17], have been

widely used to model the cellular responses to environment changes.

It is well known that cell's interaction with extracellular matrix depends on the forces generated within the actin cytoskeleton (CSK) and applied to the extracellular matrix through focal adhesions [18,19]. As a result, cells can sense physicochemical and biochemical signals that transmit between cell and substrate, and balance generated forces between internal and external cell.

A computational model based on tensegrity structure is developed to mimic how the cell probes the stiffness of a substrate and makes relative strain energy changes in this study. This study is based on the assumption that the cell can guide its movement by probing the substrate rigidity. Our assumption is that cells prefer to stay in lower energy state and move in a way to decrease its internal energy when it is probing the substrate stiffness in different directions. In the following section, the previous research results and computational models are briefly discussed to give an insight on the cellular responses due to the environment changes. The model description and the fundamental equations for the relationship of the strain energy with the substrate rigidity will be introduced. Results and discussions about the morphological changes and variations in strain energy due to the different substrate stiffness and prestress values will be given in the subsequent section.

2 Literature Review

2.1 Background Overview

Cells' alterations in shape and structure caused by mechanical loads are critical to cell functions, such as growth, motility, differentiation, and proliferation [20,21]. It is also well known that cells' directional movements are important components of developmental patterning, wound healing and tumor metastasis [22,23]. It is a critical question to understand the mechanisms by which the cells resist and react to the deformation under various physical conditions.

The forces generated within the actin cytoskeleton and applied to the extracellular matrix through focal adhesions can influence cell activities with extracellular environments, such as cell migration and formation of focal adhesion [18,19]. Focal adhesion is a molecular complex formed at the place where cell adhesion to the substrate, which is as known "mechanosensor". Cell can sense physicochemical and biochemical signals of surrounding environments which can be transmitted between cell and substrate via focal adhesions. By probing environment parameters or connecting with environment directly, cells can guide their activities due to the environmental changes, such as changing morphologies and migratory directions. The *in-vitro* studies [24, 25, 26] have shown that cells cultured on substrate are influenced by substrate mechanics. Georges *et al.* [24] showed that cells are able

to sense the substrate rigidity since certain types of cells have less rounded shape on stiffer substrate, and are more likely to exhibit as rounded shape on softer substrate. In the study of Saez *et al.* [25], they got the opposite results by using epithelial cells - cells are likely to extend into branched morphologies on softer substrate than the same cells on stiffer substrate. Cell morphology was changing, but they migrated towards the area of larger stiffness. Previous experiments also have shown that cells tend to move towards stiffer region on certain patterned substrate, which is known as durotaxis [26]. Substrate stiffness varies across cell types, from softer brain tissue to stiffer bone tissue. The differences in substrate stiffness are caused by the various substrates' components and their concentrations.

To get better understanding of these complex structures and processes, various mechanical computational models have been developed in recent decades [27, 28,29,30,31,32,33]. Mechanical computational models could give insights into how the physical properties of the substrate or adherent cells influence cells' morphologies and movements. There are two main categories of computational models to investigate cells' responses to environmental changes: continuum approach [27,28,29,30] and micro/ nanostructral approach [27,31,32,33]. An overview of the developed computational models summarized in Figure 2.1.

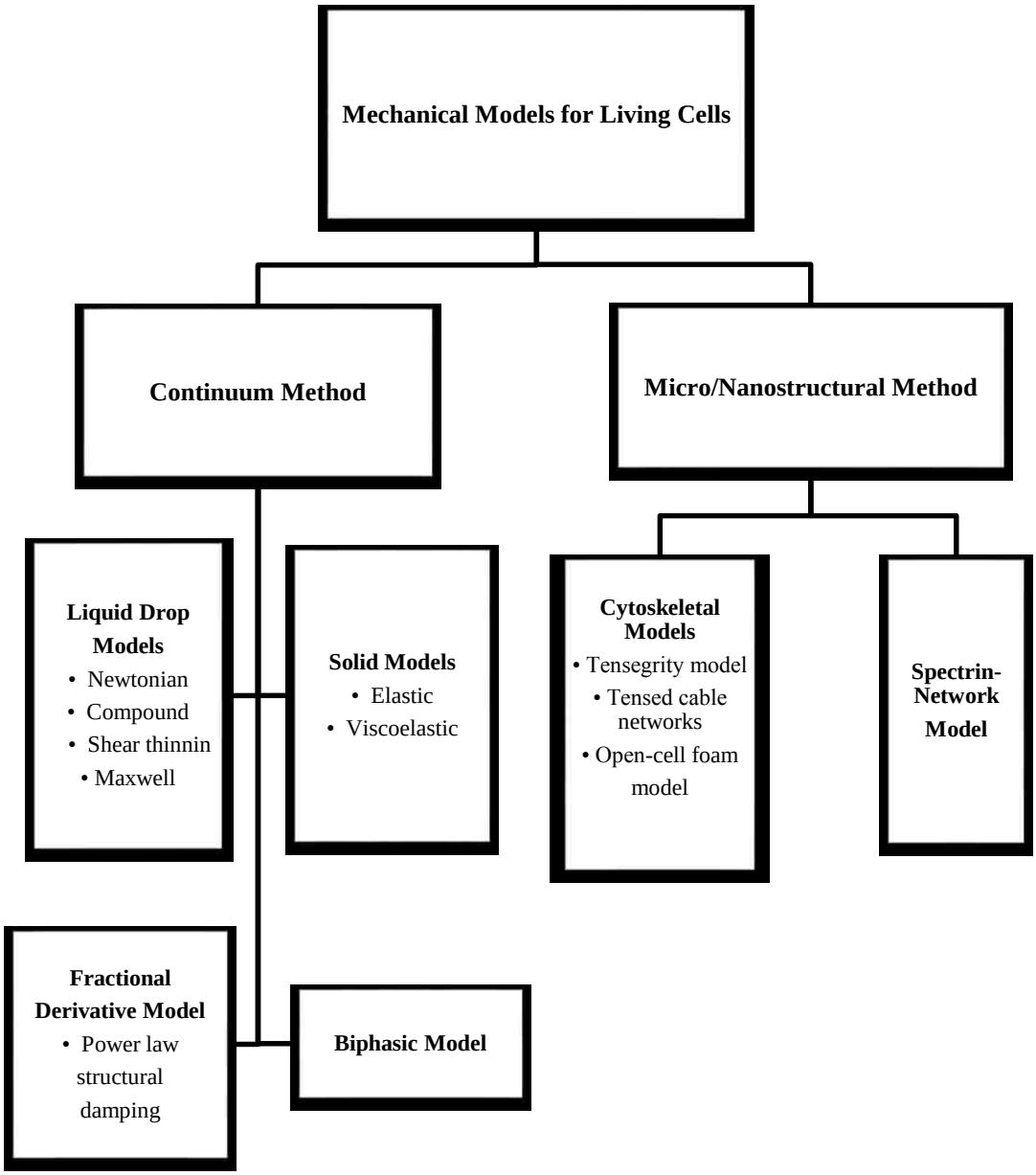

Figure 2.1 An overview of the computational models for living cells

The first category of computational model can be defined as continuum mechanical model that includes four major different types: liquid drop model, power-law structural damping model, solid model, and biphasic model. The cells are treated as certain continuum material properties in this method. The continuum mechanical model has been used to model blood cell with cytoplasm as a viscous liquid and

cortex as cortical membrane [28], to study small strain deformation characteristics of leukocytes as a linear viscoelastic solid model [29] and to model single chondrocytes and their interaction with the extracellular cartilage matrix [30].

The second category of computational model is based on microstructural and nanostructural approach. This approach includes the tensegrity model, tensed cable network model, open-cell foam model and spectrin-network model for erythrocytes. The cytoskeleton is used as the main structural component in microstructural and nanostructural approach, especially for developing cytoskeletal mechanics in adherent cell [27]. Prestressed cable network model is used to model the deformability of the adherent cell actin cytoskeleton based on the values observed from living cells and mechanical measurements on isolated actin filaments [27]. Another type of model – open-cell foam model – can be categorized into two types. The first type of open-cell foam model is used to evaluate the mechanical properties and homogenized behaviors of the foam [31,32,33]. However, on the basis of this model it is found that the bulk modulus and hydrostatic yield strength of real foams usually are over predicted. To circumvent this drawback, various morphological defects (e.g., non-uniform and wavy cell edges) have to be included [34]. The other one called “super-cell model” has been developed in order to give a better representation of the morphological structure of real foams which usually contain a number of irregular cells, especially Voronoi model, which has been developed by Gibson and her co-workers [35,36]. Among microstructural and nanostructural approaches, tensegrity model that is in

conjunction with the finite element method is the one most widely used. The tensegrity architecture was first described by Buckminster Fuller in 1961[37]. The basic idea of tensegrity model has explained the stress-hardening taking into account internal tensions [38].

2.2 Tensegrity Model

Tensegrity structure consists of a set of interconnected filament members carrying compression or tension to provide a mechanical force balance environment, stable volume and shape in the space. The tensegrity structure is used to explain cell motility and shape changes since it provides a comprehensive approach based on a fact that the mechanical integrity is maintained and a self-equilibrium is obtained through the contribution of actin filaments that are under tension and microtubules that are under compression [39,40]. The general tensegrity structure with 3 nodes fixed is represented in Figure 2.2. The structural principle of tensegrity structure is based on the use of isolated components in compression inside of a net of connected tension components in order to separate the compressed members from each other. The role of tension elements (e.g., cables) carrying “prestress” (i.e., initial stress) is to confer load-supporting capability to the entire structure. The compression elements (e.g., struts) provide prestress in the tension elements. Several models basing on tensegrity architecture have been used to successfully predict the mechanical responses of whole cells, such as the erythrocyte membrane and viruses [38].

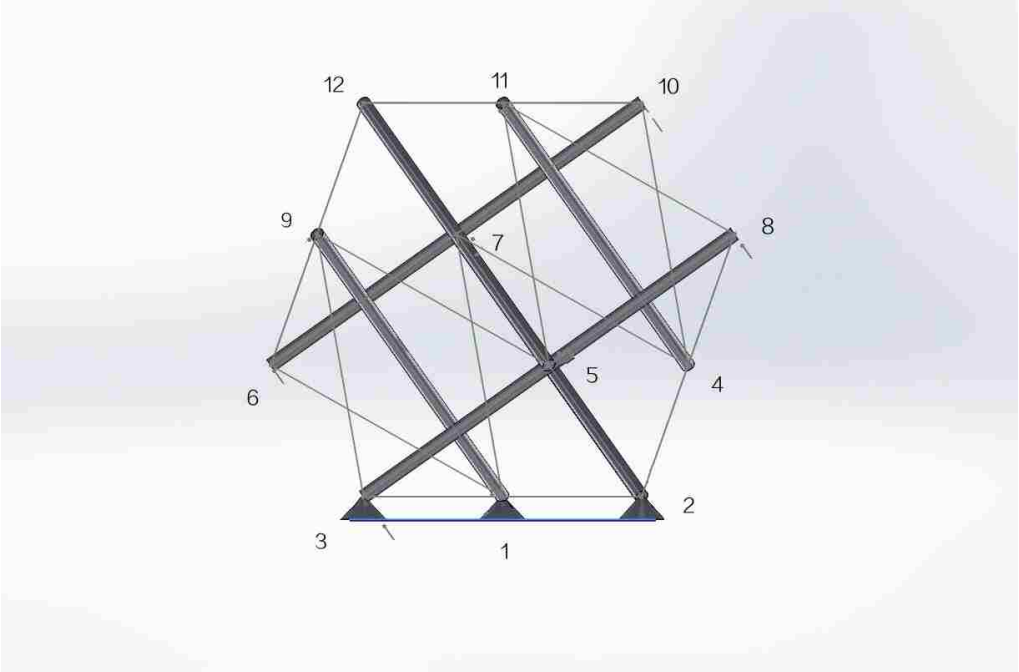

Figure 2.2 A tensegrity structure anchoring to a substrate. The thin lines represent microfilaments; the thick gray lines (struts) indicate microtubules. The line at the bottom represents the substrate, marked by triangle nodes showing the focal adhesions - the possible adhesion sites of cell-substrate system.

In previous studies, researchers concluded that tissues may act continuously under macroscopic scale, but in fact, they are discrete structural entities when viewed at the scale of cell [41]. The cells also prefer to form attachments heterogeneously that distribute over the cell surface discretely [42]. Tensegrity structure can appropriately model such characteristics. Tensegrity structure has been developed as a computational model of cell-substrate system and explains the dependency of cell activities on substrate rigidity. When a cell attaches to a particular surface, geometry of cell changes as if external forces are applied to the cell membrane. Thus, mechanotransduction reflects the reaction of the cell to the external mechanical effects. Cellular responses are variable and give rise to a variety of changes of

morphology and movement. Study of structure interactions between the cell and the substrate will provide an insight for understanding related molecular mechanisms. Cell's morphology and movement that adheres to a substrate is determined by the internal strain energy and interfacial energy. Our assumption is that cell can probe its external environment and guide its movement. When cells probe the substrate stiffness in different direction, they will find a direction that results in the decrease of the internal strain energy since they prefer to stay in a lower energy state [43,44].

In this study, we evaluated the effects of substrate stiffness on the strain energy of a spreading cell. The cytoskeleton of a cell is modeled as a tensegrity structure with prestress and its strain energy is calculated using finite element methods based on the stiffness of substrate which it attached to.

3 Simulation Description

3.1 Simulation Tool – ANSYS Mechanical APDL

ANSYS Mechanical APDL is a software developed by ANSYS, Inc., (Canonsburg, PA, USA). ANSYS Mechanical APDL offers a comprehensive finite element analysis for structural studies. The product provides a complete set of element behaviors, material models and equation solvers for a wide range of engineering problems. In this study, we use ANSYS Mechanical APDL to develop a static analysis. The geometry generates directly from ANSYS Mechanical APDL. The graphical user interface of ANSYS Mechanical APDL is presented in Figure 3.1.

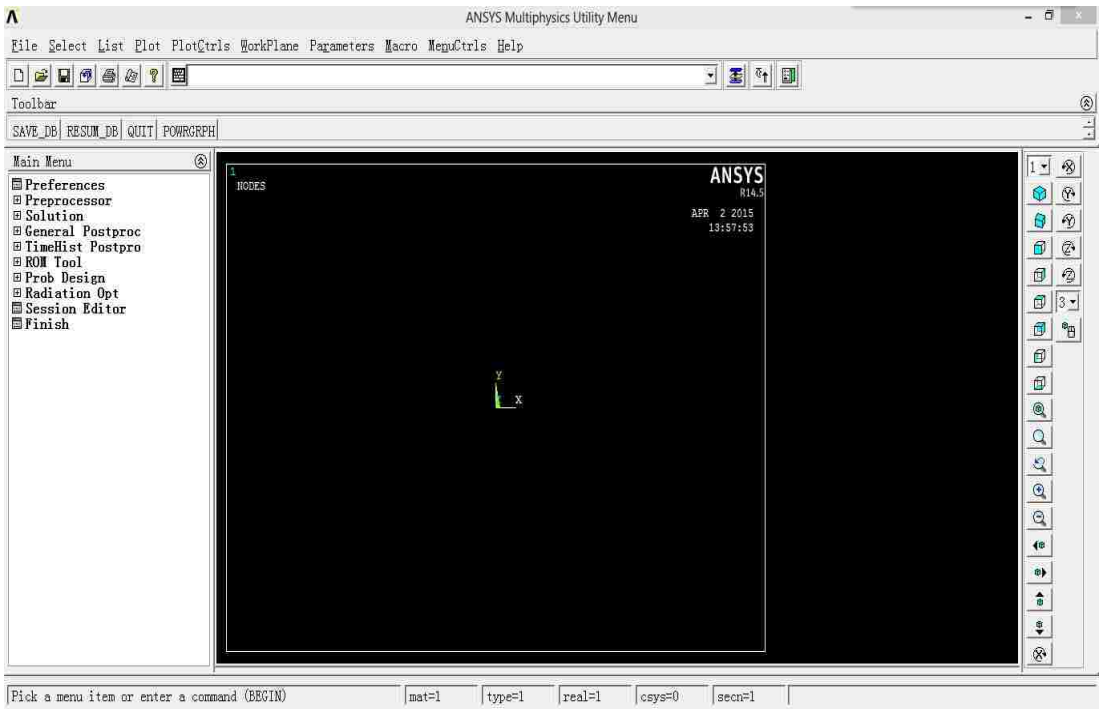

Figure 3.1 GUI of ANSYS Mechanical 14.5R

3.2 Model Description

In this study, the cytoskeleton of a living cell is represented by a tensegrity structure, while the substrate is assumed to be a plane with a specific stiffness. The model is stable due to the fact that tensile and compressive components are at all times in mechanical equilibrium. This mechanical equilibrium results from the way the compression and tensile components interact: the cables pull in on both ends of the struts, while the struts push out and stretch the cables.

3.2.1 Geometry

The tensegrity structure representing cell consists of 30 elements. Such structure may represent a 3T3 cell. 3T3 cells come from a cell line established in 1962 by George Todaro and Howard Green [45]. 3T3 cells were obtained from mouse embryo tissue. There are 6 pre-compressed struts that represent microtubule members under compressional loads. The rest 24 elements are pre-tensed cables that are homologous with microfilament members that carry tensional loads. A spring element (between nodes 2 and 13) is used to model an elastic substrate that cytoskeleton is anchored to via focal adhesion. Polydimethylsiloxane (PDMS) is the basic material for cell substrate fabrication in the *in-vitro* studies. The substrate we use to model is fabricated by such material. The model is shown in Figure 3.2. Node 3 is the origin of the coordinate system, node 1 is fixed.

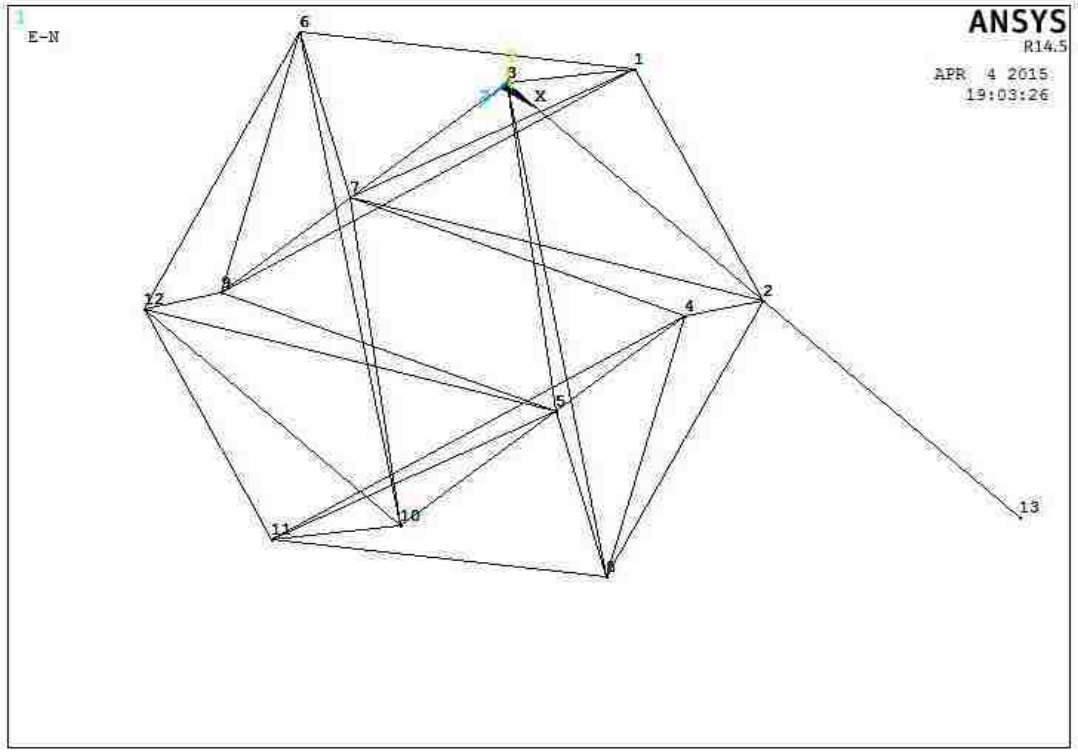

Figure 3.2 Tensegrity Model with Spring Element (nodes 2-13) Representing the Substrate Stiffness.

Twelve nodes are connected by cables and struts. Node 2 represents focal adhesion, which is linking the substrate and cell. The nodes are allowed to move in three dimensional space without rotation, representing the active movement of a living cell. The length of cable or strut is allowed to increase or decrease in this model as a function of the applied prestress and external deformation. The initial length of microtubule and microfilament are 10 μm and 6.12 μm, respectively. The original height of the tensegrity structure representing the cell is 8.7 μm. The distance between the so-called "superior plane" (the farthest plane respect to X-Y plane) and the "inferior plane" (the nearest plane respect to X-Y plane) for undeformed structure is

the initial height and these two planes were set to be parallel to each other in the initial state. The initial model is anchored to a flat substrate.

3.2.2 Material Properties of the Elements

To model the cell, we choose Link 180, Beam 188 and Combine 14 as element components from the ANSYS elements library. Link 180 and Beam 188 are three dimensional truss elements. In ANSYS, there is no need to mesh the truss elements. Thus, we do not have meshing process in this study. Link 180 element is used to model the cable system that we set up in this study, while Beam 188 element is used to model the strut system. All components of basic model are treated as elastic. Material properties for microtubules and microfilaments are not known precisely, they can be estimated from previous source. In Gittes *et al.* [46] study of the thrice-cycled phosphocellulise-purified tubulin, the Young's modulus was found to be 1.2 GPa for microtubules and 2.6 GPa for microfilaments, the Poisson's ratio for microtubules and microfilaments is 0.3. Tubulin was thought to be specific to eukaryotic cell, 3T3 cells that were obtained from mouse embryo tissue were also a kind of eukaryotic cell. Thus, we use these values as our elements' material properties (Table 3.1).

Table 3.1 Material and Mechanical Properties of Microtubules and Microfilaments

	Microtubules	Microfilaments
Element Type in ANSYS APDL	Link 180	Beam 188
Cross-section Area[46] (μm^2)	1.9×10^{-4}	1.9×10^{-5}
Length (μm)	10	6.12
E[46] (GPa)	1.2	2.6
ν[46]	0.3	0.3

Combine 14 is spring-damper element has longitudinal capability in three dimensional applications. Since Combine 14 has only longitudinal capability, we do not need to consider the bending or torsion of the element. The longitudinal spring-damper is a uniaxial tension-compression element with up to three degrees of freedom at each node: translations in the nodal X, Y, and Z directions. Table 3.2 shows the properties of Combine 14 element.

Table 3.2 Material and Mechanical Properties of Substrate

	Substrate
Element Type in ANSYS APDL	Combine 14
Original Length (μm)	6.12
Stiffness (N/m)	Varies

In this study we model attachments of the cell to surfaces with various stiffness values via focal adhesion. Since substrates vary from cell types and its components, stiffness of substrate is changeable. In the study of Trichet *et.al* [47], they chose flat

PDMS substrate to investigate REF52 fibroblast cell migration response to the stiffness gradients of the substrate. The stiffness of substrate ranges from 0.003 N/m to 1.4 N/m. In another study, Gray *et al.*[48] have evaluated two different substrates: acrylamide and PDMS. The values of substrate Young's moduli in this study were 2.5 ± 0.2 MPa and 12 ± 1 kPa for PDMS material. The cross section area of each material substrate was approximately 10 mm × 50 mm, while the height was 1mm. Stiffness can be calculated by using Young's modulus and its structure: K = (AE) / L, where A = cross sectional area, L = length, and E is Young's modulus. The stiffness value of PDMS substrate in this study is between 2.6 N/m to 540 N/m. Even though the main material of substrate is PDMS, various concentrations of PDMS lead to substrates with different rigidities. The flexural rigidity of substrate was assigned in the range of 10^{-3} to 1000 N/m and the values selected for analysis are presented in Table 3.3.

Table 3.3 Substrate Stiffness Range

Model	Stiffness (N/m)	Model	Stiffness (N/m)
1	0.001	**14**	0.09
2	0.002	**15**	0.1
3	0.004	**16**	0.2
4	0.006	**17**	0.3
5	0.008	**18**	0.4
6	0.01	**19**	0.5
7	0.02	**20**	1
8	0.03	**21**	5
9	0.04	**22**	10
10	0.05	**23**	50
11	0.06	**24**	100
12	0.07	**25**	500
13	0.08	**26**	1000

3.3 Governing Equations

Due to mechanical coupling between the cell and substrate, the change of substrate rigidity will mediate the cell morphology and migration through the assembling or disassembling process of focal adhesion. Since applied prestress force balances by tension and compression elements, the lengths of struts or cables are changed and the whole structure deforms in order to achieve new force equilibrium. Thus, we model the axial force (F_i) for ith cable or strut element to be of the following form:

$$F_i = E_i A_i \frac{\Delta L_i}{L_i}, \tag{1}$$

where E_i is elastic modulus, A_i is area of cross section, ΔL_i is change of length in ith element, L_i is original length for ith element.

The stiffness (K_i) of cable or strut represents its the ability to deform (ΔL_i) in response to applied force (F_i), thus stiffness can be described by the following relationship:

$$K_i = \frac{F_i}{\Delta L_i}. \tag{2}$$

By combing Equation (1) and (2), we obtain the relationship between stiffness and its structural properties:

$$K_i = \frac{E_i A_i}{L_i}. \tag{3}$$

Mathematically, the displacement of each node can be expressed as follows:

$$[K]\{D\} = [L], \tag{4}$$

where $[L]$ is load of each element nodal, $[K]$ is the stiffness coefficient of each

element nodal, and $\{D\}$ is the displacement of each element nodal.

The strain energy (E) stored in each cable and strut can be contributed by the elastic response in the cell can be then effectively expressed as follows:

$$E = E_c + E_s$$
$$= \frac{1}{2}\int_V \boldsymbol{\sigma_{ci}}^T \boldsymbol{\varepsilon_{ci}}\, dV + \frac{1}{2}\int_V \boldsymbol{\sigma_{si}}^T \boldsymbol{\varepsilon_{si}}\, dV\ , \quad (5)$$

where E_c denotes the energy stored in cables, and E_s denotes the energy stored in cables. $\boldsymbol{\sigma_{ci}}$ and $\boldsymbol{\varepsilon_{ci}}$ are the components of stress and strain of each cable, while $\boldsymbol{\sigma_{si}}$ and $\boldsymbol{\varepsilon_{si}}$ are the components of stress and strain of each strut respectively.

3.4 Initial Constraints and Prestress

3.4.1 Initial Constraints

In the initial state, only node 1 is constrained in all degrees of freedom (translation and rotation), while the rest twelve nodes are constrained only in rotational freedom. Node 1 is anchored in the substrate to represent focal adhesion between the cell and substrate.

In every simulation we modify stiffness of the substrate by selecting various values for the spring element stiffness. Node 1 is constrained in all translational degrees of freedom during the simulation process, while the other nodes can move in all three directions. Initial constraints in each step of the analysis also involve application of an initial prestress to the microtubule and microfilament elements in the model.

3.4.2 Prestress

Cellular prestress has a structural importance in resisting extracellular forces and maintaining cell morphology. If there is an external load acting on the structure, the components of structure move relative to one another until attaining a new equilibrium between cell and external environment. The cytoskeleton prestress plays a key role in mechanotransduction [46]. Gardel *et al.*[49] assumed that the cells' mechanical properties, especially cell prestress, can influence cells' deformation. The critical importance of prestress makes the model even more similar to the behavior of living cells as the degree of prestress determines the cells stiffness. Therefore, it is necessary

to apply prestress forces into cytoskeleton modeling. In this study, prestress values assigned to microfilament and microtubule elements of model are varied to study their effects on the cell strain energy (Table 3.4). The values represent different cases of the prestress of 3T3 cell.

Table 3.4 Prestress Value Range

Prestress Case Number	Microfilament (pN)	Microtubules (pN)
1	1.6	3.92
2	1.0	3.92
3	2.2	3.92
4	1.6	3.42
5	1.6	4.42

3.5 Simulation Process

The gravity and magnetic fields are neglected in the simulation. The model includes possibility of focal adhesion. By extending one of the nodes, the cell can probe and sense the stiffness rigidity of substrate. The strain energy of the cell changes when it extends one of the nodes in order to probe the stiffness of the substrate. This strain energy is computed at number of stiffness values. We model the substrate stiffness by a spring element. In our model, the displacement of the node attached to the substrate and total strain energy of the whole cell will be used to explain the cell preference to move to a stiffer substrate.

The simulation process is performed as follows. The first step is to apply prestress force to the structure. The length of struts or cables will change according to the internal force changes. The location of each node in the tensegrity structure is redefined due to the changes of node location in every step. The deformed location of each node in the first step has been stored and used as the new initial location for the second step of the cell simulation. The second step is to give both node 2 and the other side of spring element (node 13) an equal displacement in X direction. We apply equal displacement of node 2 and the node of the other side of spring element (node 13) to assure that there is no force in the spring element. Therefore the spring element will not influence the cell remodeling until the third step. The equal displacement was selected to be 1 μm. Since the length of each element in the model is greater than the displacement, the shape of cell will not change significantly due to this displacement.

The location of each node has been stored as the initial location for the third step. In the second step, we also get the reaction forces at node 2 which were generated due to the displacement in X direction from ANSYS directly. In the third step we fix one side of the spring element (node 13) and apply the reaction force that was calculated in the previous step at the site of node 2 in X direction, and then simulation process ends. In this step, the total strain energy of the cell is calculated and stored in the database. The schematic of the analysis is presented in Figure3.3.

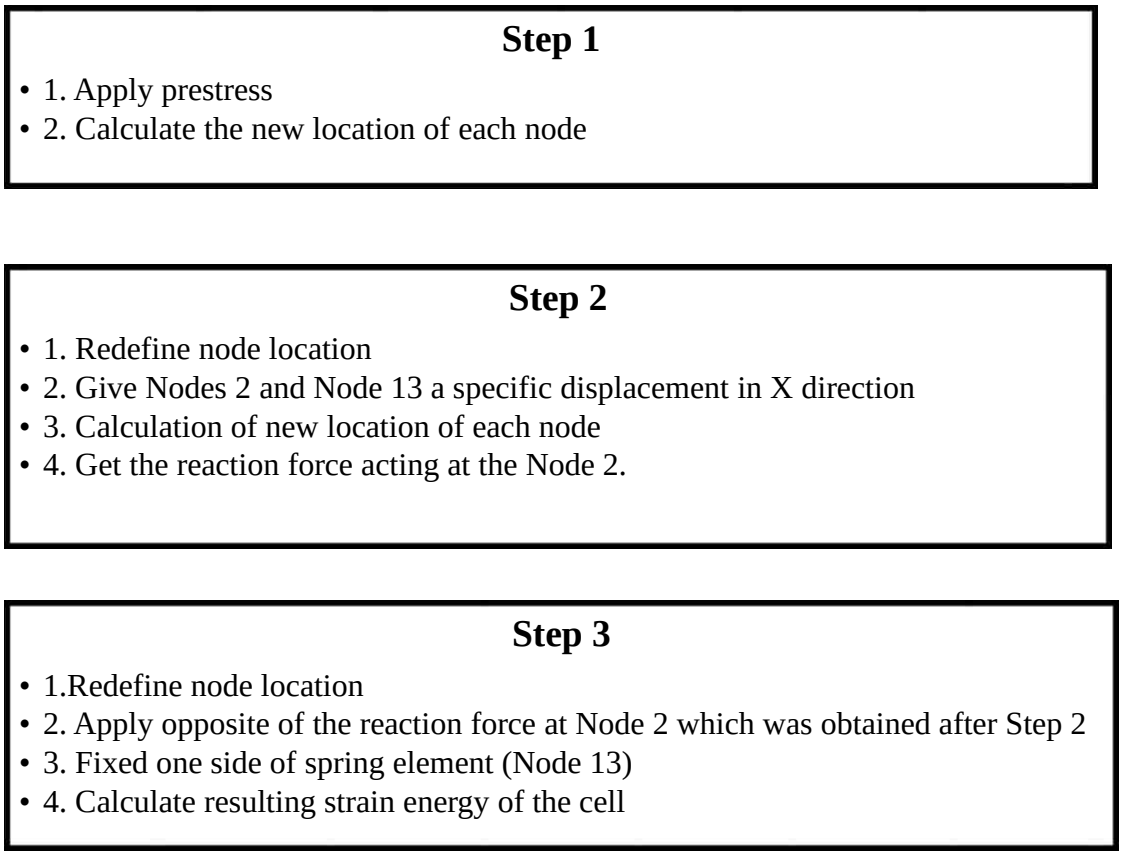

Figure 3.3 Flow Chart of the Simulation Process

4 Results and Discussions

To understand the relationship between preferential direction of cell movement and substrate stiffness during spreading process, the cytoskeletal model was placed on a particular substrate with a certain stiffness. To evaluate the influence of the prestress on cell preferential direction while cell is anchored on a particular substrate, the model was solved for different values of prestress forces. Simulations were performed on flat substrate which has no topological preference since there are no other factors that guide the cell motion in a preferential direction. Hence, the direction of cell motion is defined by analyzing substrate rigidity and cell prestress only. To evaluate the potential of cell directional movement, we used tensegrity system as a model. The cell was anchored to the substrate with different stiffness values.

4.1 Influence of the Substrate Rigidity on the Cell Energy

By running the model with ANSYS Mechanical APDL solver, the tendency of cell movement with different substrate rigidity was analyzed. To explore the relationship between substrate stiffness and cell directional movement with the certain prestress values of cable and strut elements, number of different values of substrate stiffness had been used in this study. Since the PDMS substrate stiffness in previous experimental study of Trichet *et.al* [47] and Gray *et al.* [48] was in the range of 0.003

N/m and 540 N/m, the stiffness of spring element that presents substrate ranges from 10^{-3} to 10^{3} N/m in this study. The applied prestress values of the model structure were selected to be 1.6 pN for microfilaments and 3.92 pN for microtubules (Case 1).

We increment the substrate stiffness as shown in Table 3.3. The displacements of each node were around 10^{-7} m after applying prestress. Since lengths of the cables and the struts are around 10^{-6} m, the location of each node changed very little after the first step (application of prestress). The deformation of cell structure after the second step has been shown in Figure 4.1. It is obvious that the node 2 and node 13 moved the same prescribed distance. We prescribed a 1 μm displacement in X direction in this step (Figure 4.1). The spring element (between node 2 and node 13) has no internal force until the third step. In the second step, we also get the reaction forces at node 2 due to the applied displacement. Other nodes have less displacement except those nodes that were directly connected with node 2 by cable or strut element.

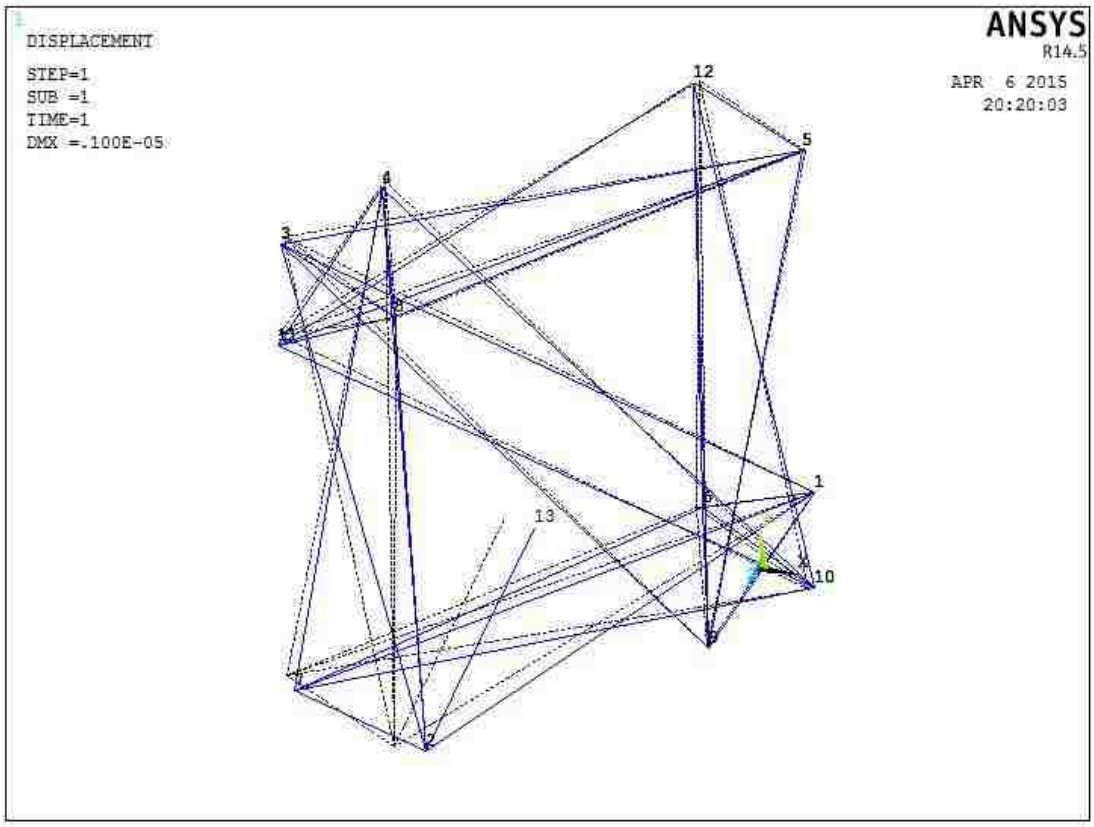

Figure 4.1 Deformation Comparison after the 2nd Step. It is obvious that the segment 2-13 just translated but did not change its length.

The deformation comparison of the whole cell model before and after the third step has been shown in Figure 4.2. The short dash line shows the structure before the third step, while the solid line shows the structure after the third step. For the third step, the node 13 is located at the same location since the node 13 (one side of the spring element) is fixed. The node 2 displaced 8.78×10^{-7} m in X direction since the substrate rigidity is very small, just 0.001 N/m (Figure 4.2). Soft spring element represents soft substrate rigidity, which is more flexible. Under a specific situation, soft substrate rigidity can lead to large deformation and strain energy change of whole cell.

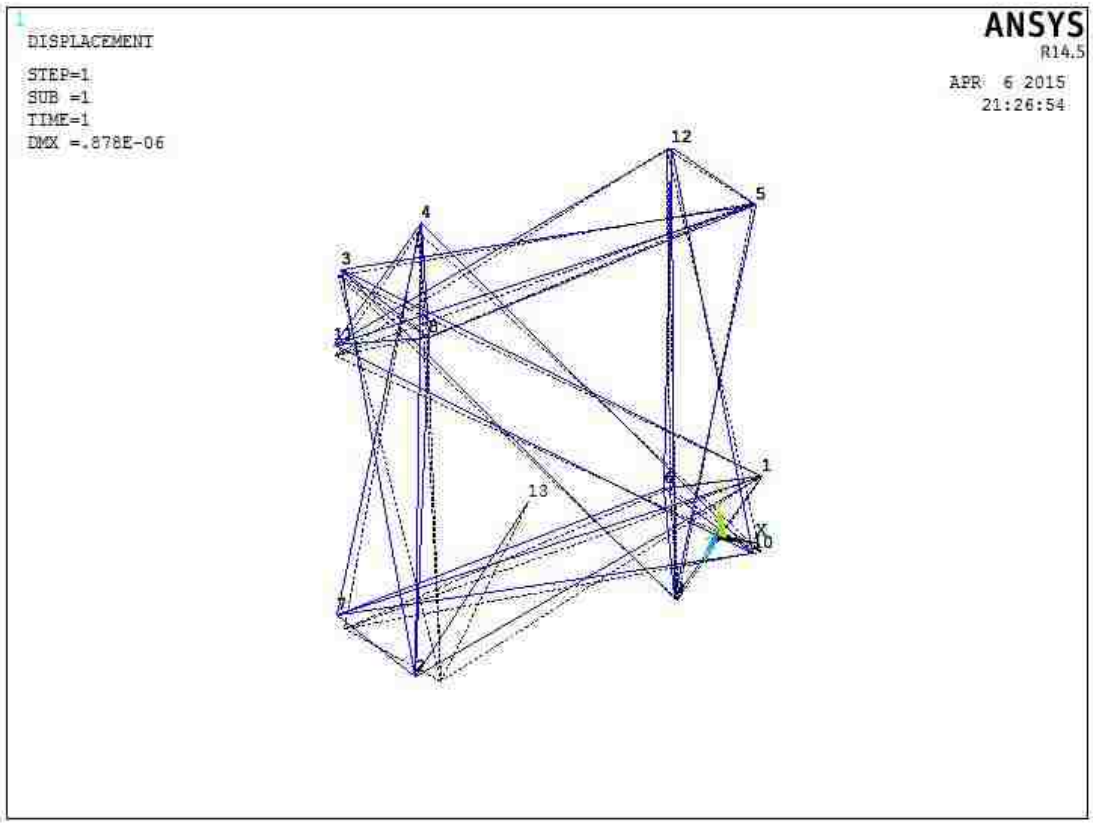

Figure 4.2 Deformation Comparison after the 3rd Step

The case of substrate rigidity equals to 0.001 N/m shows how the simulation process works for a particular substrate rigidity.

The displacement of node 2 and strain energy of cell has been influenced by substrate stiffness. The simulation results of model that were for the first case of prestress values and different substrate stiffness values are shown in Table 4.1.

Table 4.1 Strain Energy and Node 2 Displacement in X Direction for the Substrate Stiffness in the range of 10^{-3} N/m to 10^{3} N/m (Prestress Case 1)

Model	Substrate Stiffness (N/m)	Displacement of Node 2 in X direction (m)	Strain Energy ($\times 10^{-20}$ J/m^2)
1	0.001	8.78×10^{-7}	33800
2	0.002	7.73×10^{-7}	26200
3	0.004	6.25×10^{-7}	17130
4	0.006	5.24×10^{-7}	12060
5	0.008	4.51×10^{-7}	8940
6	0.01	3.96×10^{-7}	6900
7	0.05	1.15×10^{-7}	585
8	0.1	6.11×10^{-8}	166.0
9	0.5	1.28×10^{-8}	9.31
10	1	6.46×10^{-9}	3.90
11	5	1.30×10^{-9}	2.14
12	10	6.50×10^{-10}	2.09
13	50	1.30×10^{-10}	2.07
14	100	6.51×10^{-11}	2.07
15	500	1.30×10^{-11}	2.07
16	1000	6.49×10^{-12}	2.07

Since the range of stiffness values is large, Figure 4.3 and Figure 4.4 are using logarithmic scale for stiffness values. The results of displacement of node 2 in X direction with different substrate stiffness have been shown in Figure 4.3. We found that the displacement of node 2 is a function of substrate stiffness. With the substrate stiffness increases, the displacement of node 2 decreases significantly.

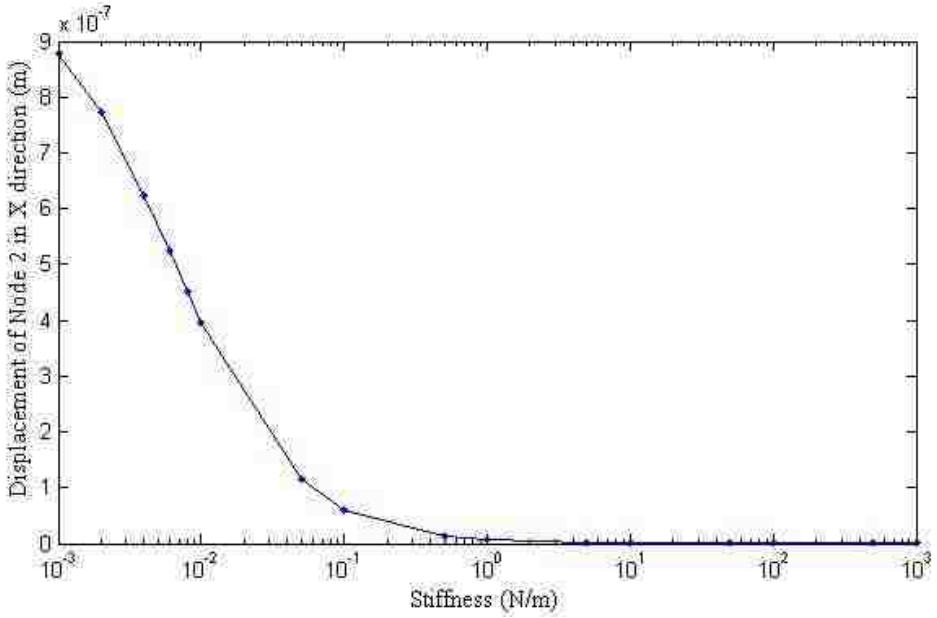

Figure 4.3 Displacement of Node 2 after the 3rd Step in X direction for Substrate Stiffness in the range of 10^{-3} N/m to 10^{3} N/m (Prestress Case 1)

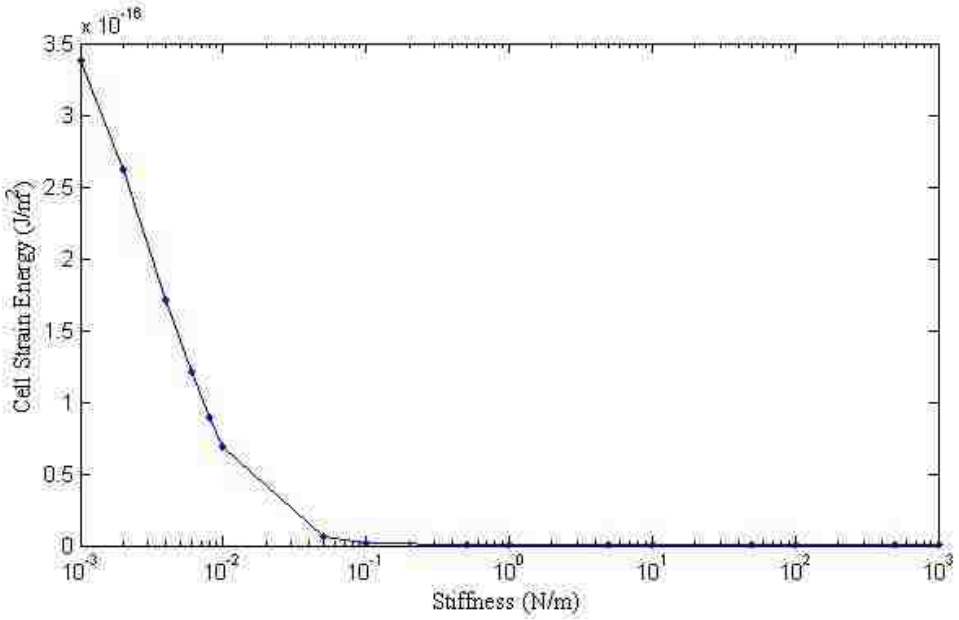

Figure 4.4 Cell Strain Energy for Substrate Stiffness in the range of 10^{-3} N/m to 10^{3} N/m (Prestress Case 1)

The total cell strain energy that includes both cable and strut elements is presented in Figure 4.4. When the substrate stiffness becomes more than 0.5 N/m, the

cell strain energy tends to change very little (Figure 4.4), while the displacement of node 2 in X direction keeps decreasing (Figure 4.3).

There is a significant change in the elastic energy when substrate stiffness in a range between 0.001 N/m and 0.05 N/m (Figure 4.4). In order to visualize the changes of the elastic energy in the range of stiffness from 0.001 N/m to 1000 N/m, the results in narrower stiffness ranges are shown in Figure 4.5, 4.6, 4.7 and 4.8. In order to show this great decreasing change, several values of substrate stiffness have been added into between 0.001 N/m and 0.05 N/m. The related results are shown in the Table.1 in Appendix.

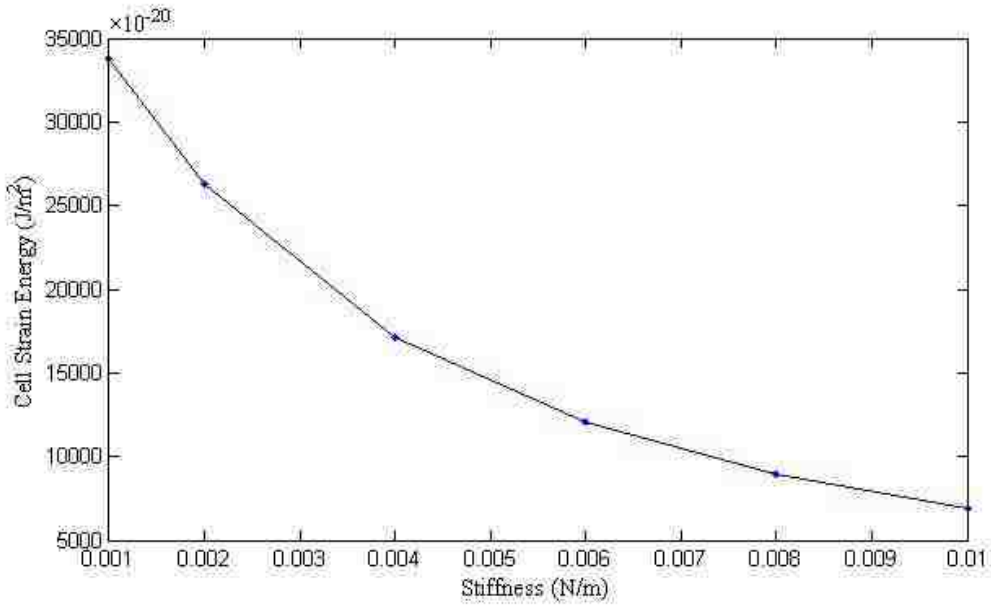

Figure 4.5 Cell Strain Energy for Substrate Stiffness in the range of 0.001 N/m to 0.01 N/m (Prestress Case 1)

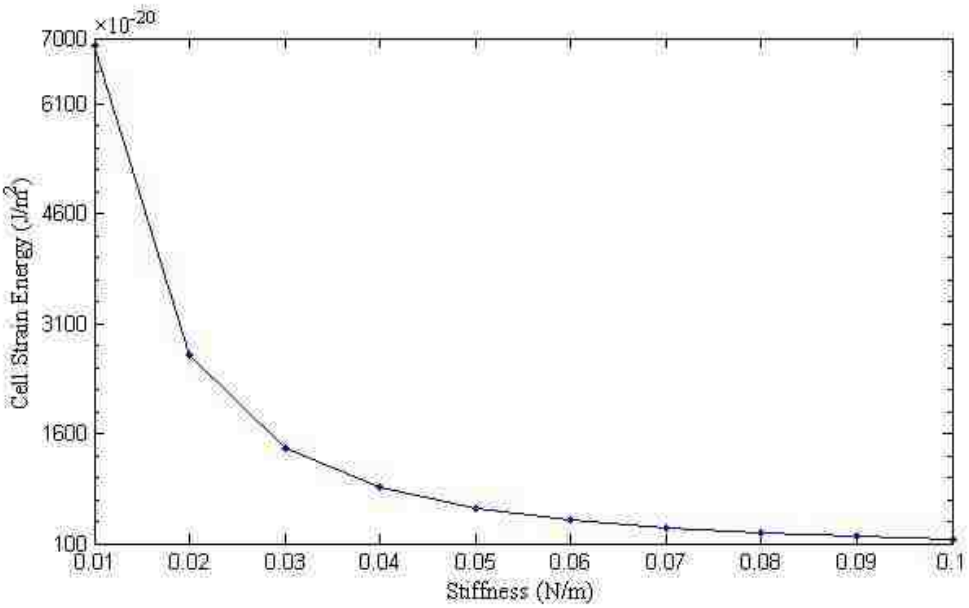

Figure 4.6 Cell Strain Energy for Substrate Stiffness in the range of 0.01 N/m to 0.1 N/m (Prestress Case 1)

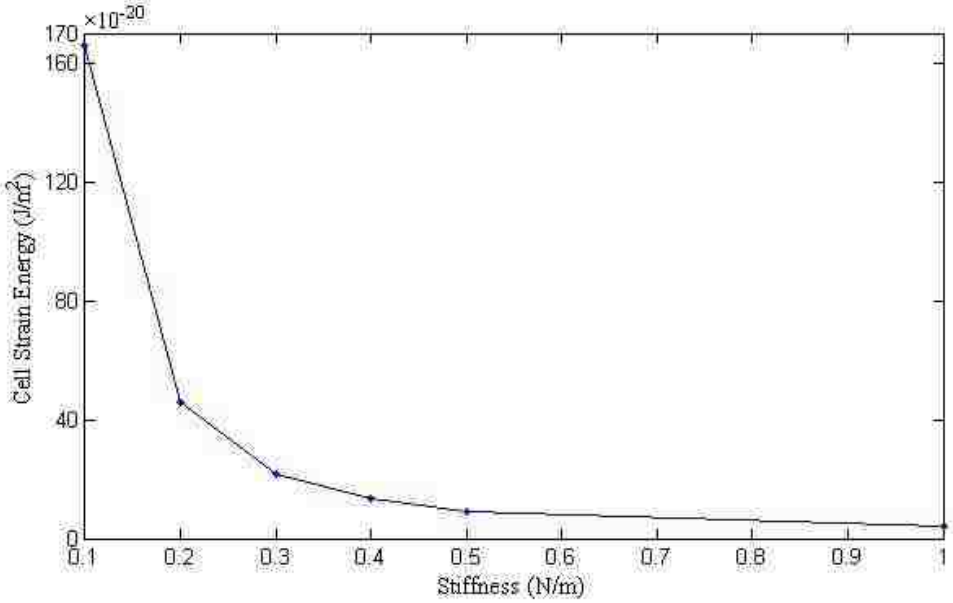

Figure 4.7 Cell Strain Energy for Substrate Stiffness in the range of 0.1 N/m to 1 N/m (Prestress Case 1)

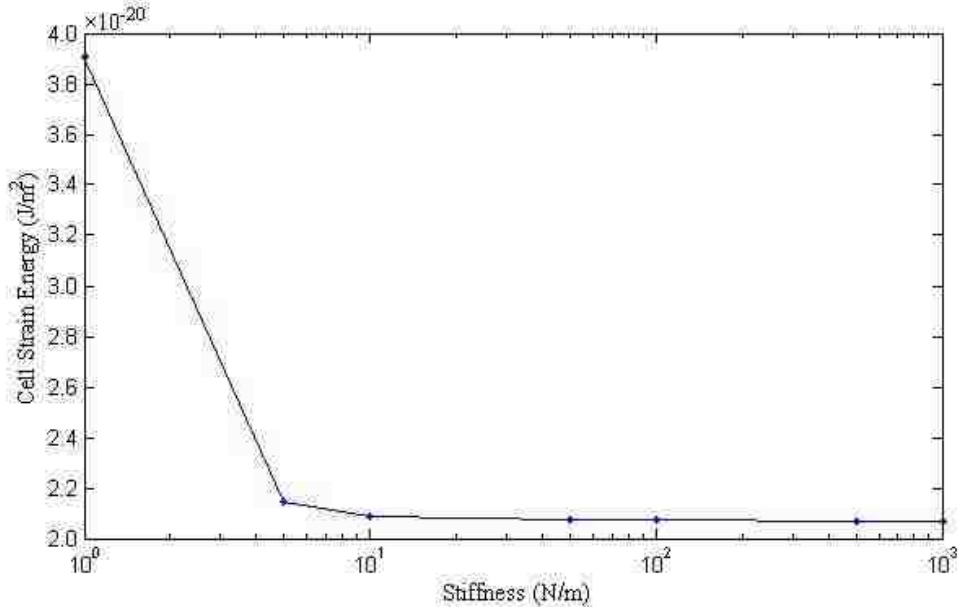

Figure 4.8 Cell Strain Energy for Substrate Stiffness in the range of 1 N/m to 1000 N/m (Prestress Case 1)

It is evident that the cell strain energy changed greatly within the range of substrate rigidity between 0.001 N/m and 1000 N/m (Figure 4.5, 4.6, 4.7 and 4.8). The strain energy values changed from 10^{-16} J/m^2 to 10^{-19} J/m^2 when substrate stiffness was in the range of 0.001 N/m and 0.5 N/m. After substrate stiffness becomes 0.5 N/m and higher, the strain energy values are around of 2 to 9×10^{-20} J/m^2. However, the strain energy keeps decreasing with the increase of the substrate stiffness.

The displacement of node 2 in X direction decreases significantly with the increasing substrate stiffness (Table 4.1 and Figure 4.3). The results also indicate that the decrease in displacement correlates with the decrease in the strain energy. With higher substrate rigidity, the cell can keep its morphology in a low energy state, since cell tends to have less possibility of deformation and migration. While with softer

substrate rigidity, cell has larger strain energy and higher possibility of deformation and migration.

To observe the results visually, cell deformation between the second and the third step in ANSYS GUI with different substrate stiffness has been shown in Figure 4.9 to Figure 4.13.

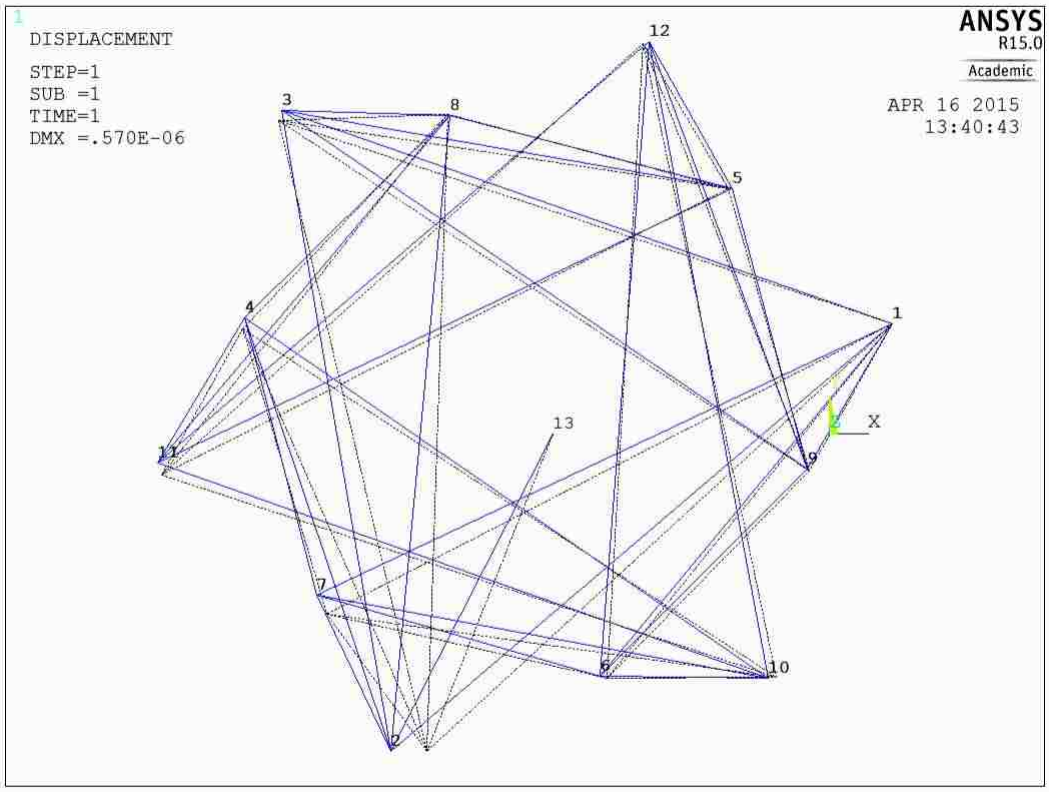

Figure 4.9 Deformation Comparison after the 3rd Step for Substrate Stiffness of 0.004 N/m (Prestress Case 1)

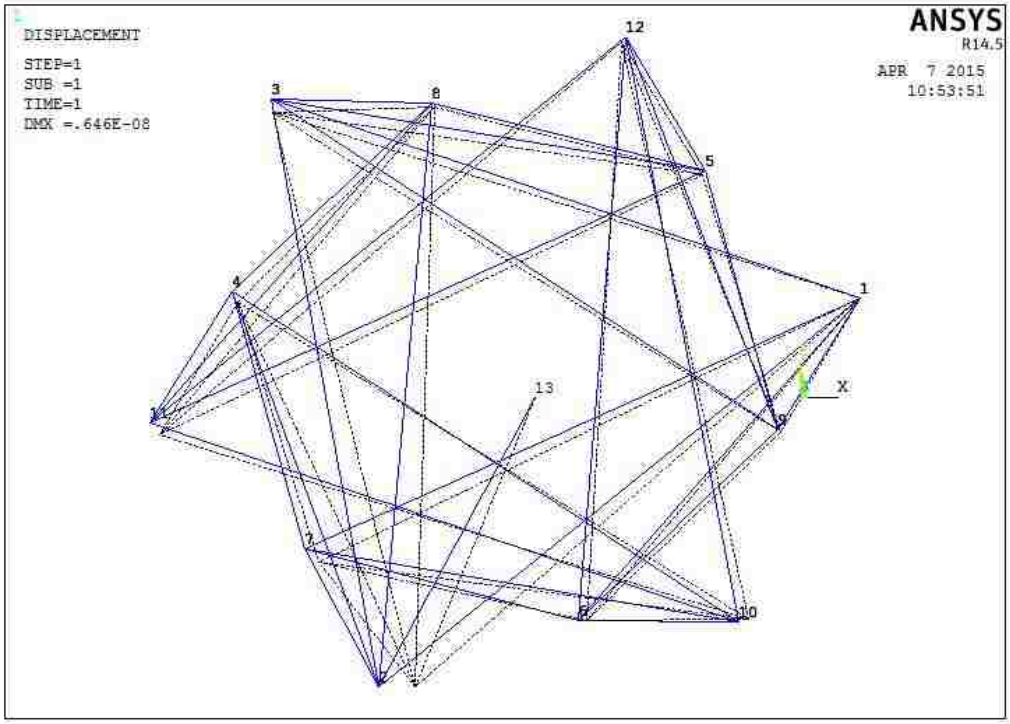

Figure 4.10 Deformation Comparison after the 3rd Step for Substrate Stiffness of 1 N/m (Prestress Case 1)

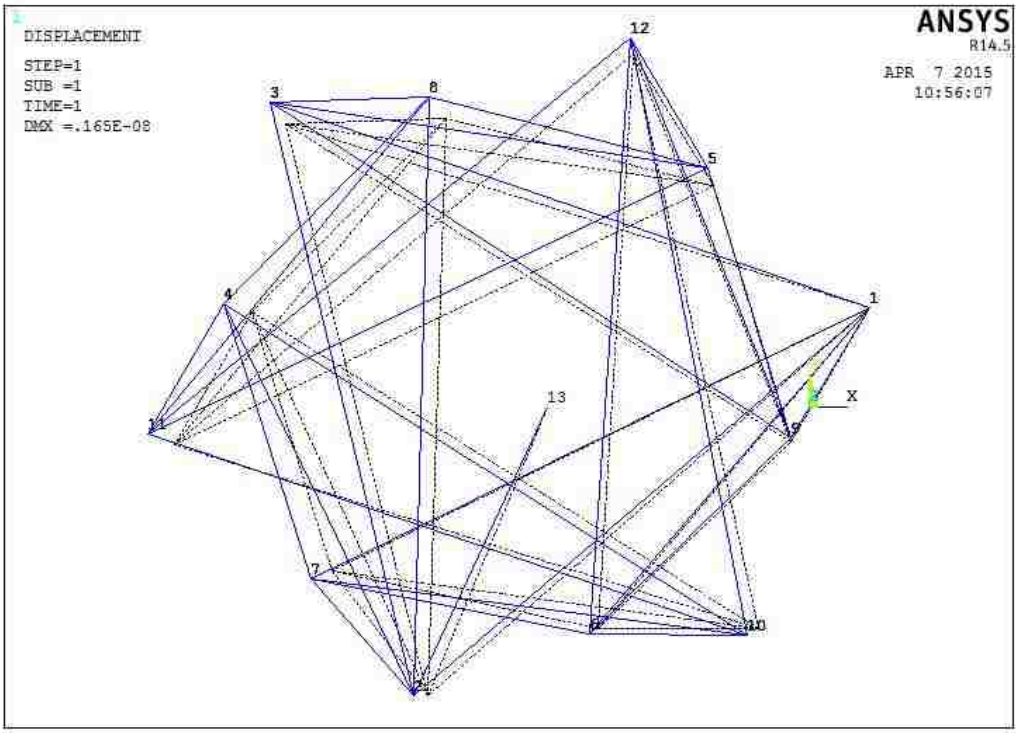

Figure 4.11 Deformation Comparison after 3rd Step for Substrate Stiffness of 10 N/m (Prestress Case 1)

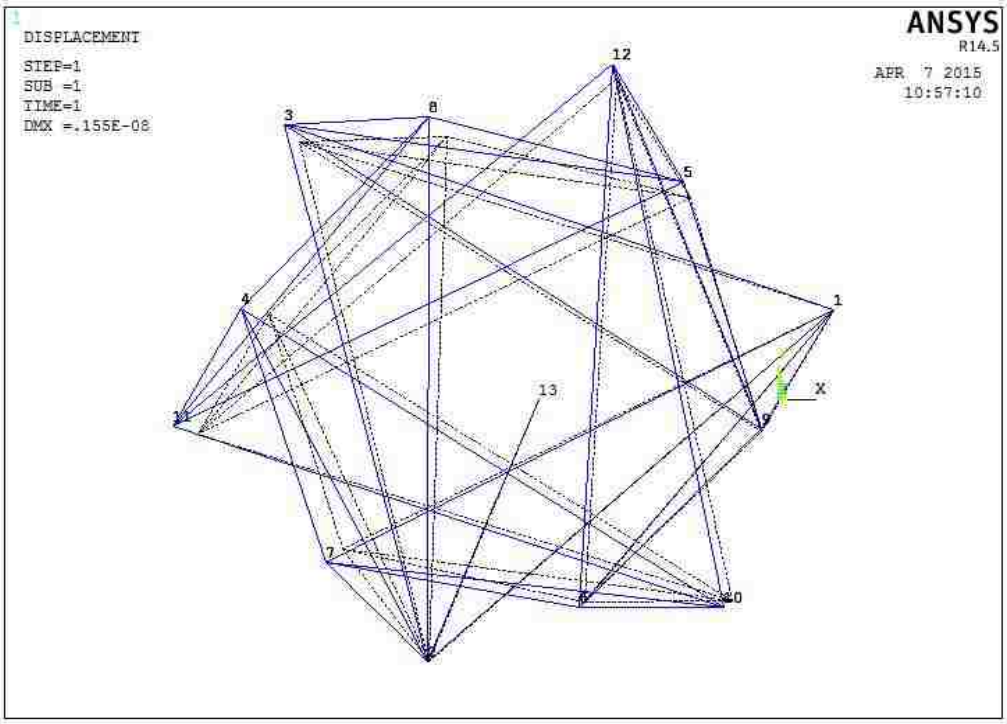

Figure 4.12 Deformation Comparison after the 3rd Step for Substrate Stiffness of 100 N/m (Prestress Case 1)

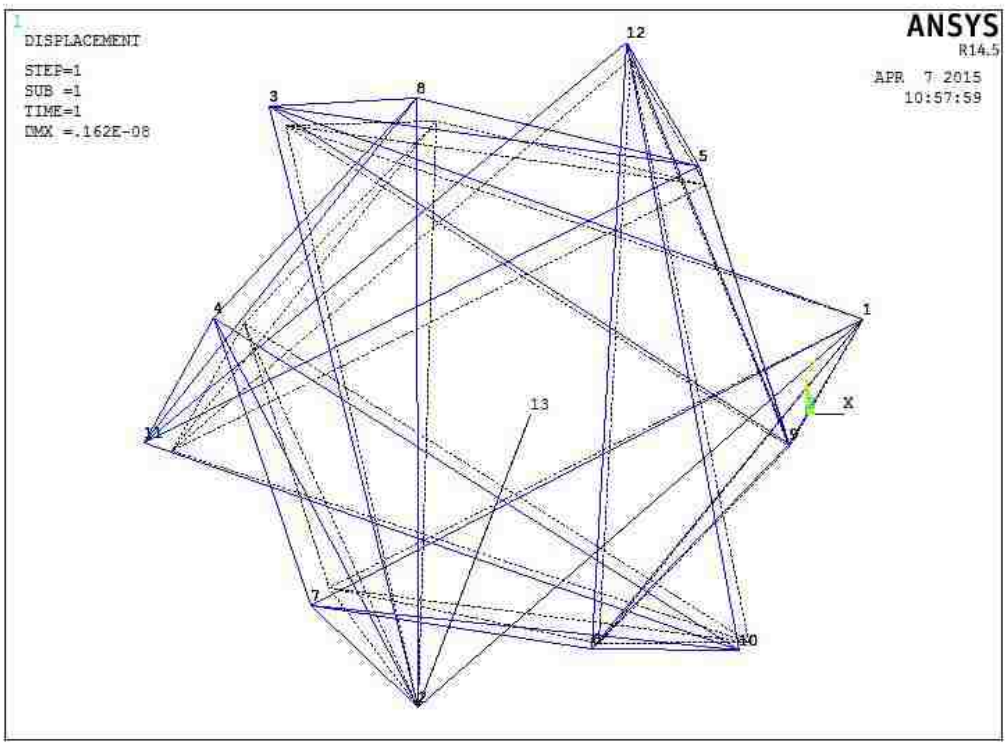

Figure 4.13 Deformation Comparison after the 3rd Step for Substrate Stiffness of 1000 N/m (Prestress Case 1)

In Figures 4.9 to 4.13, the dash line represents the cell structure we got at the second step, while the solid line presents the structure we calculated at the third step. Comparing these two images (Figures 4.9 and Figure 4.10), it is not easy to observe the change of the distance between these two lines. In Figure 4.9, the distance between the dash line and the solid line at node 2 can be seen directly from figure, it means that the displacement of node 2 before and after the third step is relatively large. The distances between dash line and the solid line at node 2 become smaller when the substrate stiffness increases, which means that the displacement of node 2 in X direction before and after the third step is smaller when substrate stiffness increases. In Figure 4.13, line between node 2 and node 13 virtually did not move. It shows that when stiffness equals to 1000 N/m, the displacement of node 2 before and after the third step is very small. The values of displacement at node 2 in X direction are 6.25×10^{-7} m for 0.004 N/m, 6.46×10^{-9} m for 1 N/m, 6.5×10^{-10} m for 10 N/m, 6.51×10^{-11} m for 100 N/m, and 6.49×10^{-12} m for 1000 N/m (Table 4.1). Although we cannot observe the displacement difference between stiffness equals to 0.004 N/m and stiffness equals to 1 N/m from Figure 4.9 and 4.10 directly, the value of displacement at node 2 is different. When the rigidity increases, the displacement of node 2 becomes smaller and cell structure has less possibility to migrate and deform comparing to the deformed structure after the second step. Therefore, the strain energy of the cell caused by deformation becomes smaller as well.

In sum, the strain energy of cell structure decreases when substrate stiffness increases and this may explain why cell tends to move towards the stiff substrate instead of the soft one.

4.2 Influence of the Prestress on the Cell Energy

To explore how the prestress influences cell strain energy and movement, we studied several cases of prestress forces with different substrate rigidity. Since we have two elements (struts and cables) loaded by prestress, we investigate the influence of each of the elements separately. First, we keep the prestress of strut element constant and change the prestress of the cable elements. In this situation, case 1, case 2 and case 3 have been studied with the prestress force of strut element equals to 3.92 pN while the prestress force values of cable element were 1.6 pN, 1.0 pN, and 2.2 pN, respectively. Then, we keep the cable elements' prestress values constant and change the prestress of strut element. The strut element prestress values were 3.92 pN, 3.42 pN, and 4.42 pN. These values have been explored in case 1, case 4, and case 5. The substrate stiffness values range from 0.004 N/m to 1000 N/m. Figure 4.14 and Figure 4.15 show the tendency of cell strain energy of case 1-3 and of case 1, case 4 and case 5 separately. In all prestress cases, the strain energy of the cell decreases when substrate rigidity increases. The prestress does not change the qualitative behavior of strain energy of cell

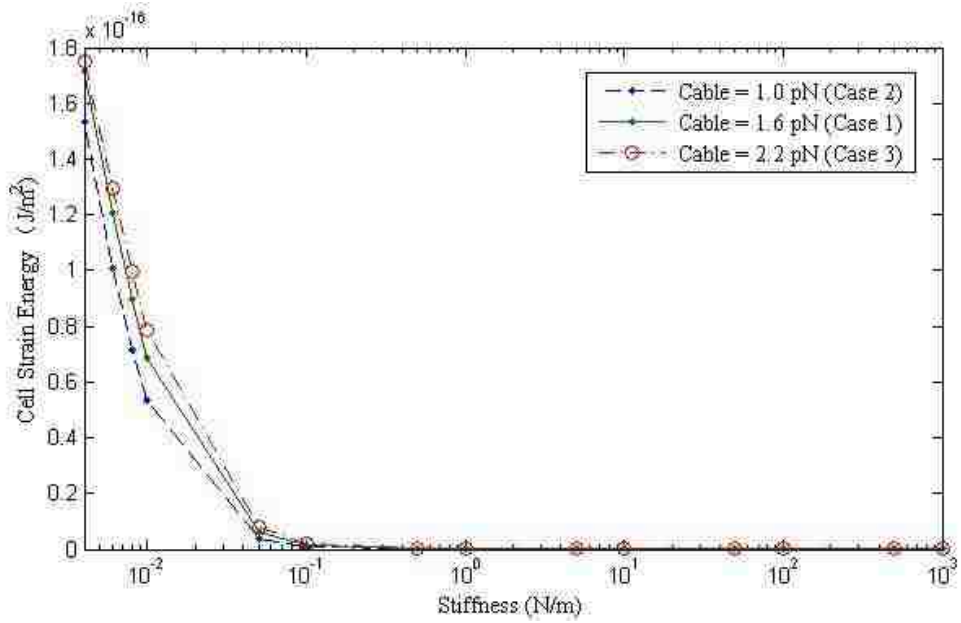

Figure 4.14 Cell Strain Energy with Prestress Cases 1, 2, and 3

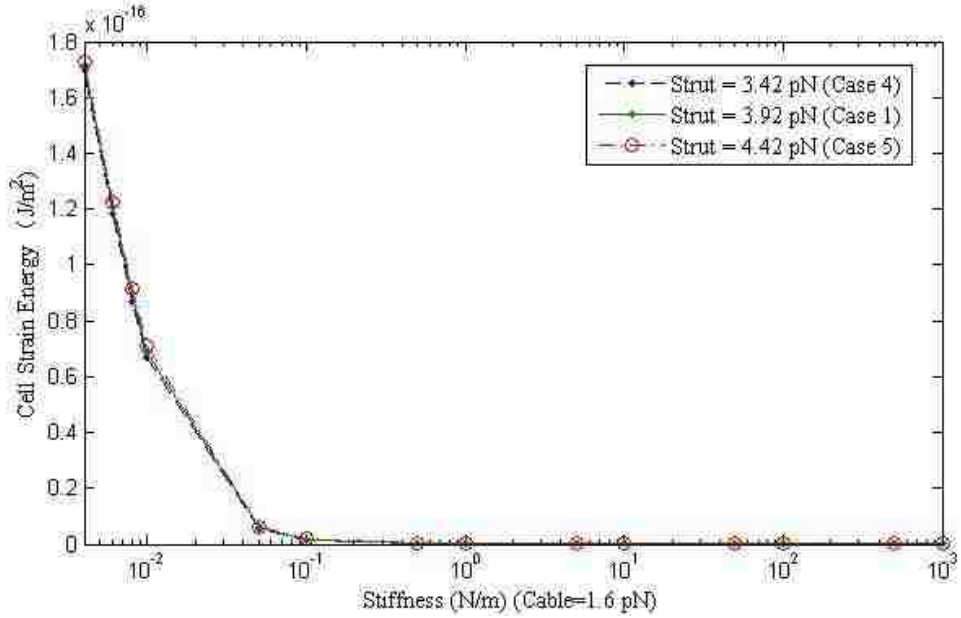

Figure 4.15 Cell Strain Energy with Prestress Cases 1, 4, and 5

The numerical difference of strain energy for the case 1-3 with three different cable prestress is significant, but qualitatively it follows the same pattern (Figure 4.14). The related results are presented in Table.2 in the Appendix. When substrate rigidity equals to 0.004 N/m, the strain energy with three different cable prestress is

1.53×10^{-16} J/m^2 for cable prestress equals to 1.0 pN, 1.71×10^{-16} J/m^2 for cable prestress equals to 1.6 pN and 1.75×10^{-16} J/m^2 for cable prestress equals to 2.2 pN respectively (Table.2). With substrate rigidity increase, the strain energy of each case tends to decrease. After substrate stiffness equals to 0.1 N/m, the differences of strain energy of these three cases become small (Figure 4.14). When substrate rigidity equals to 1000 N/m, the strain energy values are 7.61×10^{-21} J/m^2, 2.07×10^{-20} J/m^2, and 4.57×10^{-20} J/m^2 with cable prestress equals to 1.0 pN, 1.6 pN and 2.2 pN. The increasing cable prestress value gives rise to increase the strain energy of cell. With substrate stiffness increase, the strain energy of the cell tends to decrease, the change of prestress of cable element does not change behavior pattern of the strain energy.

The differences of strain energy of with three different strut prestress are small (Figure 4.15). The related results are presented in Table.2 in the Appendix. When substrate rigidity equals to 0.004 N/m, the strain energy of each strut value is 1.70×10^{-16} J/m^2 for strut prestress equals to 3.42 pN, 1.71×10^{-16} J/m^2 for strut prestress equals to 3.92 pN, and 1.73×10^{-16} J/m^2 for strut prestress equals to 4.42 pN, respectively. Since the value of strain energy in each case is small, the differences are not obvious (Figure 4.15). When strut elements have larger prestress, the strain energy of the cell is larger accordingly. When substrate rigidity equals to 1000 N/m, the strain energy values are 1.94×10^{-20} J/m^2, 2.07×10^{-20} J/m^2, and 2.21×10^{-20} J/m^2 corresponding to the strut prestress equals to 3.42 pN, 3.92 pN and 4.42 pN. When stiffness of substrate becomes larger, the strain energy of the cell tends to be smaller. The results of strain

energy when substrate stiffness equals to 500 N/m and 1000 N/m are both 2.21×10^{-20} J/m^2 when prestress of strut elements equals to 4.42 pN. It does not reflect the strain energy change precisely due to the calculation accuracy of the finite element procedure. The strain energy is continuing to change, however the change is quite small. Hence, the change of prestress value does not change behavior pattern of the strain energy: the strain energy will decrease with substrate stiffness increase.

4.3 Discussions

This study is based on the assumption that the cell can guide its movement by probing the substrate rigidity. Since from the mechanical point of view it is preferable to be in a lower energetic state, we assume that while probing the substrate stiffness in different direction cell will find a direction that results in the decrease of the cell's internal elastic energy and will move in this direction. Experimental observations confirm that cells can probe their environment through lamellipodial extensions [50,51] and guide their movement with substrate stiffness [52,53]. As the substrate rigidity increasing, the cell has smaller internal strain energy, leading to directed movement onto the rigid substrate. Conversely, as substrate becomes softer, the strain energy of cell structure increases. We have mentioned [11,19] that mechanical force generated between substrate and cell regulates the deformation and migration of the cell. This is to be expected in an active sensing system of cell-substrate system, because the force or deformation will influence the cell and substrate interactions. In most cases cells move towards the substrate where the substrate is stiff, and away when the substrate is soft. In Ni and Chiang's study [43], they developed a mathematical model to demonstrate how substrate rigidity influences cell migration and morphology. The cell was assumed as two-dimensional flat elastic membrane while the substrate was assumed as three-dimensional elastic structure. They demonstrated that the strain energy of cell generated by intracellular and extracellular forces destabilizes the cell morphology and migration activity. In the other words, with substrate stiffness increase

the lower energy state of cell can be reached. In order to get minimal strain energy state, cell would migrate from the region with lower stiffness to the region with higher stiffness. In our study, when the strain energy is large, cell has higher possibility to migrate to the position where they can reach the minimal strain energy. These results confirm our results based on tendency of cell movement. The related experimental results are presented by Lo, Wang, Dembo, and Wang [10] in the study of National Institutes of Health 3T3 cells and culturing them on flexible polyacrylamide sheets coated with type I collagen. In this study, they controlled material concentrations to create high and low rigidity regions in one substrate sheet. The result showed that the overall rate migration of cells increased significantly as the cell crossed the rigidity boundary from the soft to the stiff side. The cells' preferential migration direction is a stiff region. The experimental observation clearly indicates that our assumption that the cell prefers movement in the direction of a stiffer substrate, based on its internal elastic energy corresponds to the substrate stiffness.

The physicochemical and biochemical of external environment signals can be detected and transduced into intracellular responses, which be capable of affecting the cell behavior via focal adhesion. Cells can sense substrate stiffness by extending a probe in particular direction, and attaching itself to the surface. On stiff substrate, cell has smaller displacement of focal adhesion since the reaction force is a function of the substrate stiffness. The stronger mechanical feedback may then lead to the stress-sensitive ion channels' activations [54] or tension-sensitive proteins' conformational

changes. The focal adhesions form easily and lead more stable system between the cell and substrate. Therefore, the cells prefer to move to stiff substrate rather than soft substrate.

In addition to substrate rigidity, we have explored possibility that prestress in cell itself also regulates the cell movement. Although the strain energy for each prestress case is different, the change of prestress value does not change behavior pattern of the strain energy: cell's strain energy will decrease when substrate stiffness increases.

In this study, the current simulation results provide direct evidences for the guidance of cell migration by substrate rigidity and prestress based on the minimization of the internal elastic energy. Related phenomena have been reported in literature review in recent decades. In reality, the cell movement is probably guided by a complex interplay among chemical and physical signals, which may include substrate rigidity as well as forces generated by other activities: fluid shear and cell-cell interactions.

5 Conclusions

We proposed a computational model based on tensegrity structure as a cell model and spring element to model the substrate. The stiffness of surface to which cells adhere has a profound effect on cells' morphology. According to the model, the stiffer is the substrate, the lower is the strain energy and smaller is the deformation of cell structure. When prestress of a cell is increased, the strain energy of the cell is increased. Since connections between cells with low strain energy and substrates are more stable, they would increase the cells' functional efficiencies and focal adhesions' formations [55]. Consequently, this would result into a directional cell motion from softer region to stiffer region on the substrate with varying rigidity.

Based on aforementioned discussions, the conclusions based on the obtained results are:

1) The substrate rigidity and cell prestress play a certain role in cell directional movement,
2) The change of prestress value does not change behavior of the strain energy: cell's strain energy will decrease with substrate stiffness increase,
3) With substrate rigidity increase, the strain energy of cell structure decreases. This tendency explains that within a substrate with various rigidity, cell prefers to move towards stiffer regions in experimental observations reported in the literature review.

The computational results show that the cell strain energy changes due to the extracellular environments and cellular prestress. By analyzing the cell response to different prestress values and substrate rigidity, it is shown that cells will move towards the position where their internal elastic energy is lower, which corresponds to the available experimental data.

Reference

1. Stamenović, D., & Ingber, D. E. (2009). Tensegrity-guided self assembly: from molecules to living cells. Soft Matter, 5(6), 1137-1145.

2. Discher, D. E., Janmey, P., & Wang, Y. L. (2005). Tissue cells feel and respond to the stiffness of their substrate. Science, 310(5751), 1139-1143.

3. Georges, P. C., & Janmey, P. A. (2005). Cell type-specific response to growth on soft materials. Journal of applied physiology, 98(4), 1547-1553.

4. Wang, N., Butler, J. P., & Ingber, D. E. (1993). Mechanotransduction across the cell surface and through the cytoskeleton. Science, 260(5111), 1124-1127.

5. Chicurel, M. E., Chen, C. S., & Ingber, D. E. (1998). Cellular control lies in the balance of forces. Current opinion in cell biology, 10(2), 232-239.

6. Ghosh, K., Pan, Z., Guan, E., Ge, S., Liu, Y., Nakamura, T., Ren, X. D., Rafailovich, M., & Clark, R. A. (2007). Cell adaptation to a physiologically relevant ECM mimic with different viscoelastic properties. Biomaterials, 28(4), 671-679.

7. Engler, A. J., Sen, S., Sweeney, H. L., & Discher, D. E. (2006). Matrix elasticity directs stem cell lineage specification. Cell, 126(4), 677-689.

8. Guo, W. H., Frey, M. T., Burnham, N. A., & Wang, Y. L. (2006). Substrate rigidity regulates the formation and maintenance of tissues. Biophysical journal, 90(6), 2213-2220.

9. Jiang, G., Huang, A. H., Cai, Y., Tanase, M., & Sheetz, M. P. (2006). Rigidity sensing at the leading edge through α V β 3 integrins and RPTPα. Biophysical journal, 90(5), 1804-1809.

10. Lo, C. M., Wang, H. B., Dembo, M., & Wang, Y. L. (2000). Cell movement is guided by the rigidity of the substrate. Biophysical journal, 79(1), 144-152.

11. Sochol, R. D., Higa, A. T., Janairo, R. R., Li, S., & Lin, L. (2011). Unidirectional mechanical cellular stimuli via micropost array gradients. Soft Matter, 7(10), 4606-4609.

12. McGarry, J. G., & Prendergast, P. J. (2004). A three-dimensional finite element model of an adherent eukaryotic cell. Eur Cell Mater, 7, 27-33.

13. Chen, T. J., Wu, C. C., Tang, M. J., Huang, J. S., & Su, F. C. (2010). Complexity of the tensegrity structure for dynamic energy and force distribution of cytoskeleton during cell spreading. PloS one, 5(12), e14392.

14. Parameswaran, H., Lutchen, K. R., & Suki, B. (2014). A computational model of the response of adherent cells to stretch and changes in substrate stiffness. Journal of Applied Physiology, 116(7), 825-834.

15. Flaherty, B., McGarry, J. P., & McHugh, P. E. (2007). Mathematical models of cell motility. Cell biochemistry and biophysics, 49(1), 14-28.

16. Wendling, S., Oddou, C., & Isabey, D. (1999). Stiffening response of a cellular tensegrity model. Journal of theoretical biology, 196(3), 309-325.

17. Coughlin, M. F., & Stamenovic, D. (1998). A tensegrity model of the cytoskeleton in spread and round cells. Journal of biomechanical engineering, 120(6), 770-777.

18. Li, S., Guan, J. L., & Chien, S. (2005). Biochemistry and biomechanics of cell motility. Annu. Rev. Biomed. Eng., 7, 105-150.

19. Sheetz, M. P., Felsenfeld, D. P., & Galbraith, C. G. (1998). Cell migration: regulation of force on extracellular-matrix-integrin complexes. Trends in cell biology, 8(2), 51-54.

20. Chen, C. S., Mrksich, M., Huang, S., Whitesides, G. M., & Ingber, D. E. (1997). Geometric control of cell life and death. Science, 276(5317), 1425-1428.

21. Bernstein, L. R., & Liotta, L. A. (1994). Molecular mediators of interactions with extracellular matrix components in metastasis and angiogenesis. Current opinion in oncology, 6(1), 106.

22. Friedl, P., Zänker, K. S., & Bröcker, E. B. (1998). Cell migration strategies in 3-D extracellular matrix: differences in morphology, cell matrix interactions, and integrin function. Microscopy research and technique, 43(5), 369-378.

23. Yeung, T., Georges, P. C., Flanagan, L. A., Marg, B., Ortiz, M., Funaki, M., Zahir, N., Ming, W. Y., Weaver, V., & Janmey, P. A. (2005). Effects of substrate stiffness on cell morphology, cytoskeletal structure, and adhesion. Cell motility and the cytoskeleton, 60(1), 24-34.

24. Georges, P. C., Miller, W. J., Meaney, D. F., Sawyer, E. S., & Janmey, P. A. (2006). Matrices with compliance comparable to that of brain tissue select neuronal over glial growth in mixed cortical cultures. Biophysical journal, 90(8), 3012-3018.

25. Saez, A., Ghibaudo, M., Buguin, A., Silberzan, P., & Ladoux, B. (2007). Rigidity-driven growth and migration of epithelial cells on microstructured anisotropic substrates. Proceedings of the National Academy of Sciences, 104(20), 8281-8286.

26. Yeung, A., & Evans, E. (1989). Cortical shell-liquid core model for passive flow of liquid-like spherical cells into micropipets. Biophysical journal, 56(1), 139-149.

27. Coughlin, M. F., & Stamenović, D. (2003). A prestressed cable network model of the adherent cell cytoskeleton. Biophysical journal, 84(2), 1328-1336.

28. Karcher, H., Lammerding, J., Huang, H., Lee, R. T., Kamm, R. D., & Kaazempur-Mofrad, M. R. (2003). A three-dimensional viscoelastic model for cell deformation with experimental verification. Biophysical journal, 85(5), 3336-3349.

29. Shieh, A. C., & Athanasiou, K. A. (2003). Principles of cell mechanics for cartilage tissue engineering. Annals of biomedical engineering, 31(1), 1-11.

30. Lim, C. T., Zhou, E. H., & Quek, S. T. (2006). Mechanical models for living cells—a review. Journal of biomechanics, 39(2), 195-216.

31. Gan, Y. X., Chen, C., & Shen, Y. P. (2005). Three-dimensional modeling of the mechanical property of linearly elastic open cell foams. International Journal of Solids and Structures, 42(26), 6628-6642.

32. Gong, L., & Kyriakides, S. (2005). Compressive response of open cell foams Part II: Initiation and evolution of crushing. International Journal of Solids and Structures, 42(5), 1381-1399.

33. Gong, L., Kyriakides, S., & Jang, W. Y. (2005). Compressive response of open-cell foams. Part I: Morphology and elastic properties. International Journal of Solids and Structures, 42(5), 1355-1379.

34. Chen, C., Lu, T. J., & Fleck, N. A. (1999). Effect of imperfections on the yielding of two-dimensional foams. Journal of the Mechanics and Physics of Solids, 47(11), 2235-2272.

35. Silva, M. J., Hayes, W. C., & Gibson, L. J. (1995). The effects of non-periodic microstructure on the elastic properties of two-dimensional cellular solids. International Journal of Mechanical Sciences, 37(11), 1161-1177.

36. Simone, A. E., & Gibson, L. J. (1998). The effects of cell face curvature and corrugations on the stiffness and strength of metallic foams. Acta Materialia, 46(11), 3929-3935.

37. Ingber, D. E. (1993). Cellular tensegrity: defining new rules of biological design that govern the cytoskeleton. Journal of cell science, 104, 613-613.

38. Luo, Y., Xu, X., Lele, T., Kumar, S., & Ingber, D. E. (2008). A multi-modular tensegrity model of an actin stress fiber. Journal of biomechanics, 41(11), 2379-2387.

39. Ingber, D. E. (2003). Tensegrity I. Cell structure and hierarchical systems biology. Journal of Cell Science, 116(7), 1157-1173.

40. Ingber, D. E. (2008). Tensegrity and mechanotransduction. Journal of bodywork and movement therapies, 12(3), 198-200.

41. Sander, E. A., Stylianopoulos, T., Tranquillo, R. T., & Barocas, V. H. (2009). Image-based multiscale modeling predicts tissue-level and network-level fiber reorganization in stretched cell-compacted collagen gels. Proceedings of the National Academy of Sciences, 106(42), 17675-17680.

42. Cukierman, E., Pankov, R., Stevens, D. R., & Yamada, K. M. (2001). Taking cell-matrix adhesions to the third dimension. Science, 294(5547), 1708-1712.

43. Ni, Y., & Chiang, M. Y. (2007). Cell morphology and migration linked to substrate rigidity. Soft Matter, 3(10), 1285-1292.

44. Yalcintas, E. P., Hu, J., Liu, Y., & Voloshin, A. (2014). Modeling Cell Spreading and Alignment on Micro-Wavy Surfaces. CMES: Computer Modeling in Engineering & Sciences, 98(2), 151-180.

45.Todaro, G. J., & Green, H. (1963). Quantitative studies of the growth of mouse embryo cells in culture and their development into established lines. The Journal of cell biology, 17(2), 299-313.

46. Gittes, F., Mickey, B., Nettleton, J., & Howard, J. (1993). Flexural rigidity of microtubules and actin filaments measured from thermal fluctuations in shape. The Journal of cell biology, 120(4), 923-934.

47. Trichet, L., Le Digabel, J., Hawkins, R. J., Vedula, S. R. K., Gupta, M., Ribrault,

C., Hersen, P., Voituriez, R., & Ladoux, B. (2012). Evidence of a large-scale mechanosensing mechanism for cellular adaptation to substrate stiffness. Proceedings of the National Academy of Sciences, 109(18), 6933-6938.

48. Gray, D. S., Tien, J., & Chen, C. S. (2003). Repositioning of cells by mechanotaxis on surfaces with micropatterned Young's modulus. Journal of biomedical materials research Part A, 66(3), 605-614.

49. Gardel, M. L., Nakamura, F., Hartwig, J. H., Crocker, J. C., Stossel, T. P., & Weitz, D. A. (2006). Prestressed F-actin networks cross-linked by hinged filamins replicate mechanical properties of cells. Proceedings of the National Academy of Sciences of the United States of America, 103(6), 1762-1767.

50. Pelham, R. J., & Wang, Y. L. (1999). High resolution detection of mechanical forces exerted by locomoting fibroblasts on the substrate.Molecular biology of the cell, 10(4), 935-945.

51. Galbraith, C. G., Yamada, K. M., & Galbraith, J. A. (2007). Polymerizing actin fibers position integrins primed to probe for adhesion sites. Science, 315(5814), 992-995.

52. Hadjipanayi, E., Mudera, V., & Brown, R. A. (2009). Guiding cell migration in 3D: a collagen matrix with graded directional stiffness. Cell motility and the cytoskeleton, 66(3), 121-128.

53. Wong, J. Y., Velasco, A., Rajagopalan, P., & Pham, Q. (2003). Directed movement of vascular smooth muscle cells on gradient-compliant hydrogels. Langmuir, 19(5), 1908-1913.

54. Lee, J., Ishihara, A., Oxford, G., Johnson, B., & Jacobson, K. (1999). Regulation of cell movement is mediated by stretch-activated calcium channels. Nature, 400(6742), 382-386.

55. Lazopoulos, K. A., & Stamenović, D. (2008). Durotaxis as an elastic stability phenomenon. Journal of biomechanics, 41(6), 1289-1294.

APPENDIX

Table.1 Strain energy and node 2 displacement in X direction for the substrate stiffness in the range of 0.001 N/m and 1 N/m (Case 1)

Model	Stiffness (N/m)	Deformation at Node 2 in X direction(m)	Strain Energy ($\times 10^{-20} J/m^2$)
1	0.001	8.78×10^{-7}	33800
2	0.002	7.73×10^{-7}	26200
3	0.004	6.25×10^{-7}	17130
4	0.006	5.24×10^{-7}	12060
5	0.008	4.51×10^{-7}	8940
6	0.01	3.96×10^{-7}	6900
7	0.02	2.46×10^{-7}	2660
8	0.03	1.79×10^{-7}	1402
9	0.04	1.40×10^{-7}	864
10	0.05	1.15×10^{-7}	585
11	0.06	9.79×10^{-8}	423
12	0.07	8.51×10^{-8}	320
13	0.08	7.53×10^{-8}	251
14	0.09	6.75×10^{-8}	202
15	0.1	6.11×10^{-8}	166.0
16	0.2	3.15×10^{-8}	46.6
17	0.3	2.12×10^{-8}	21.8
18	0.4	1.60×10^{-8}	13.31
19	0.5	1.28×10^{-8}	9.31
20	1	6.46×10^{-9}	3.90

Table.2 Strain energy for the substrate stiffness in the range of 0.004 N/m and 1000 N/m with Various Prestress Cases

Model	Stiffness (N/m)	Strain Energy ($\times 10^{-21}$ J/m^2)				
		CASE 1	CASE 2	CASE 3	CASE 4	CASE 5
1	0.004	171300	153400	175200	169600	172600
2	0.006	120600	101000	129400	118100	122700
3	0.008	89400	71500	99400	87000	91600
4	0.01	69000	53300	78800	66700	71000
5	0.05	5850	3820	7750	5500	6200
6	0.1	16610	1050	2280	1552	1767
7	0.5	93.1	52.3	147.0	86. 8	99.5
8	1	39.0	18.90	71.4	36.5	41.7
9	5	21.4	8.07	46.7	20.1	22.8
10	10	20.9	7.73	46.0	19.60	22.3
11	50	20.7	7.62	45.7	19.44	22.1
12	100	20.7	7.61	45.7	19.43	22.1
13	500	20.7	7.61	45.7	19.33	22.1
14	1000	20.7	7.61	45.7	19.33	22.1

VITA

Jie Sheng was born on November 19, 1989 in Beijing, China. She studied Process Equipment and Control Engineering in Department of Mechanical and Power Engineering from 2008 to 2012 at East China University of Science and Technology, China. Jie Sheng completed her Bachelor of Engineering degree in July 2012. She began her graduate studies in Mechanical Engineering and Mechanics at Lehigh University since Spring, 2013. She is pursuing her MS degree under the guidance of Dr. Arkady Voloshin.